Cover Sheet

Title: *Nanostructure/Strain-Resistance in Thin Films Containing Carbon Nanofibers and Carbon Nanotubes*

Authors: Marriner Merrill

C.T. Sun

ABSTRACT

A range of nanostructured strain gages are constructed using an improved method of manufacturing nanocomposites. The manufacturing method is called Spin-Spray Layer by Layer self assembly (SSLBL). SSLbL is a variation of Layer by Layer Self Assembly (LbL), which is a water-based process capable of forming and stack nanometer thick layers, or 'nanolaminates,' of either nanoparticles or polymers simply, quickly, and inexpensively. This research utilizes the abilities of SSLbL to develop several different nanocomposites containing carbon nanofibers (CNF), multi-walled carbon nanotubes (MWCNT), or single-walled carbon nanotubes (SWCNT) to investigate how different nanostructures affect the strain-resistance response with the eventual goal of advanced strain gages. Discussion of the additional effects inherent in the strain-resistance properties of two-dimensional films compared to standard one-dimensional strain gages is presented. The experimental data from several different nanostructures with their resulting strain-resistance behavior is also presented. The highest strain gage sensitivity is found to be a film with a gage factor of 13 (zero strain) to 1560 (4% strain). Standard strain gages currently have sensitivities of about 2.0. Utilizing the experimental information, further optimization is suggested.

INTRODUCTION

One of the most exciting possibilities inherent in nanotechnology is the power to create new 'nanocomposite' materials with designed properties. Basically, this is the ability to build a material with specific electrical, mechanical, optical, or other properties. As this capability is becoming more of a reality, one of the immediate applications is in sensor technology, such as in sensing mechanical strains. Strain gage sensors are devices that have a change in a measureable property (usually electrical resistance) corresponding to a change in strain. Current strain gages are generally one-dimensional wire foil gages. While this is a very simple and

Aeronautics and Astronautics, Purdue University 701 W. Stadium Ave, West Lafayette, IN, 47907, U.S.A.

economic technology, nanostructured films could offer some greater benefits in advanced applications. For example, these nanocomposite sensors could be designed to have high sensitivity, larger elongation to failure, biocompatibility, multifunctionality, or the ability to sense strain in multiple directions simultaneously.

Recently, several researchers have developed electrically conductive nanofilms and tested them for their strain-resistance properties [1-8]. These films use conductive nanoparticles such as single walled carbon nanotubes (SWCNT), multi walled carbon nanotubes (MWCNT), carbon nanofibers (CNF), or others. There has been a wide range of properties reported, with strain sensitivities ranging from 0.1 to 50, measured for strains from 0.02% to 20% [1-4]. For a strain gage, this sensitivity or 'gage factor' is defined as the change in resistance divided by the change in strain all over the initial resistance, *i.e.*,

$$GF = \frac{\Delta R / R_0}{\Delta \varepsilon} \tag{1}$$

Most of the films developed and tested to this point fall into a few categories. The first category would be buckypaper films. Buckypaper films consist entirely of MWCNT's or SWCNT's collected into a mat. Li and Levy tested such a MWCNT buckypaper and found a sensitivity of 2-4 for up to 0.18% strain, with the ability to load and unload up to 0.045% strain with good repeatability [5]. A similar work by Reale using SWCNT buckypaper also showed good linearity. However, Reale reported a large effect that temperature can have on the response of such films, with a 15% change between tests done at 25 C and 45 C [6].

A second common type of conductive nanofilm is a blended polymer-nanoparticle film. Park recently presented results on this type of film. He mixed low volume percentages of MWCNT with polyethylene oxide using a solvent that was then evaporated. This film showed some promising results with a sensitivity of 50 at high strains (up to 7%). Interestingly, Park also showed two very distinct regions in the strain-resistance plot, with a low sensitivity (1.6-3.7) at strains less than 1%. Park explained this change by developing a simple microstructure model that indicated such things as nanotube bending, stretching, volume change, etc. [2]. Zhang, et. al prepared a film in a similar manner, with MWCNT dispersed in polycarbonate dissolved in Tetrahydrofuran. In this instance, the gage factor was somewhat higher, about 7 for strain < 1% [7].

A third, more flexible manufacturing technique, called Layer by Layer self assembly (LbL) has also been used to build polymer-carbon nanoparticle films with much higher nanoparticle loadings for strain gage testing. Loh used LbL to build films with SWCNT and double walled CNT's (DWCNT). The gage factor was fairly low, ranging from 0.1 to 0.2, though factors as high as 7.3 were reported. Loh reported some hysteresis, or change in resistance, for loading and unloading cycles. Interestingly, these films were dual purpose since they were also used to measure change in pH [1,8].

The purpose of the current work is to use SSLbL, a modification of LbL, to create a series of films with specific material differences. By producing several different films with one manufacturing process, it will be possible to make direct

comparisons in the results. While many different material properties could play a role, this research focuses on 1) the conducting nanoparticle used, 2) the method used to disperse the nanoparticles in solution and 3) the 'matrix' into which this conducting particle is placed. The second parameter is very important because the nanoparticle preparation method affects the surface of the nanoparticle and its conductivity. These in turn affect the nanoparticle dispersion and electrical percolation networks.

NANOCOMPOSITE MANUFACTURING

SSLbL Method

LbL has already been introduced as a very flexible manufacturing technique [9-12]. It is a rather simple, but slow method for building high-quality, uniform films from a broad range of different nanoparticles and polymers. Layer construction and stacking is accomplished primarily via electrostatic, positive-negative charge interactions. This is done by preparing two dilute solutions: one of an electrostatically charged nanoparticle and the other of an oppositely charged polymer. A substrate is dipped from one solution to the other with intermediate rinsing steps. At each step, the nanoparticle or polymer diffuses to the surface and attaches by charge-charge interaction. Due to the 'large' size of these colloids, the surface charge is overcome. The new surface charge repels further layer build-up and prepares for the attachment by the other solution.

Importantly, the composition of individual layers depends only on the positive or negative charge of the preceding layer, so by controlling layer composition and sequence, a nearly infinite number of different materials or devices can be built. Some reported materials assembled using LbL include photovoltaics (MWCNT, SWCNT, quantum dots) [13], electrochromics (prussian blue nanoparticles) [12], biomimetic materials (nanoclay, silver nanoparticles) [14], and structurally robust thin films (nanoclay, CNT) [15]. There are a few limitations to LbL. The process is intrinsically slow because of the diffusion step. Also, the process is wasteful of the nanoparticles because there is always some carry-over from one solution to the other, resulting in a gradual decrease in solution quality and the necessity of making new solutions after a certain number of cycles.

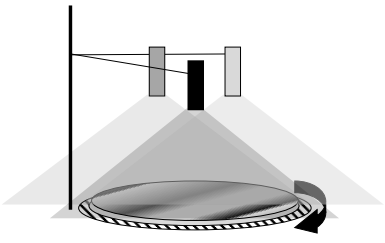

Figure 1. SSLbL schematic. The three different nozzles spray sequentially, not simultaneously.

TABLE I. LBL AND SSLBL PARAMETERS

	LbL	SSLbL
Polymer Solution Concentration	0.1% - 0.5%	0.1% - 0.2%
Particle Solution Concentration	0.1% - 1.0%	0.1% - 0.2%
Solution Volume	∞	0.5 - 4 mL
Rinse Volume	∞	4 mL
Solution Wait Time	2 – 60 min	2.5 – 4 sec
Total Cycle Time	5 – 80 min	24 – 60 sec

To overcome these obstacles, a variation of LbL has been developed called Spin-Spray LbL (SSLbL). In this method, instead of dipping the substrate in the two solutions, the solutions are sprayed directly onto a rapidly spinning substrate. So, instead of using diffusion to bring the particles into close contact with the substrate, this is done by the spinning process, which includes spinning off excess and then evaporating the remaining solvent. Using SSLbL, cycle times for Nanoparticle-Rinse-Polymer-Rinse can be decreased to less than a minute, which is more than an order of magnitude faster than traditional LbL. In addition, by carefully metering the volume of solution sprayed, it is possible to produce the films with much less waste. There is still a rinsing step so that particles or polymers which are excess but were 'trapped' on the surface by the rapid solvent evaporation can be washed off.

Table I shows the parameters for standard LbL and the corresponding SSLbL parameters. While the SSLbL parameters here are not optimized, they give the basic idea of the differences and similarities in the two systems. Figure 1 displays a simple schematic of the process.

Materials

The CNF used in this research was Pyrograf III purchased from Pyrograf Products Incorporated. The MWCNT and SWCNT were donated from Nanolabs. Laponite clay platelets were a donation from Southern Clay Products and PGV grade montmorillonite was donated by Nanocor. Both the laponite and montmorillonite platelets are expected to be 1 nm thick when fully exfoliated, but the montmorillonite is reported to have a diameter of 200-400 nm while the laponite has a diameter of only 25 nm. Sodium Dodecyl Sulfate (SDS), poly(ethylene oxide) (PEO) with MW=4,000,000, polyethyleneimine, branched (PEI) with MW=25,000, poly(sodium 4-styrenesulfonate) (PSS) with MW=1,000,000, poly(diallyldimethylammonium chloride) (PDDA) with MW=400,000-500,000 and poly(acrylic acid) (PAA) with MW=100,000 were all purchased from Sigma Aldrich. pH of the PAA and PEI solutions were adjusted, when needed, by HCl and NaOH from Sigma Aldrich. All solutions were made using generic-brand distilled water. Polymer and laponite solutions were made simply by stirring a dilute solution (0.2-1%) in water for 30 minutes. The montmorillonite solution was made by stirring 0.2% montmorillonite in water for several days, then allowing it to settle for 2 days and decanting the remaining solution.

NANOPARTICLE PREPARATION

CNF, MWCNT, and SWCNT were all used in this study. Figure 2 shows SEM micrographs of films with each of these nanoparticles. The SWCNT appears to have been heavily contaminated. There are several different methods described in the literature of dispersing carbon nanotubes or nanofibers in an aqueous solution. Because these methods directly impact the electrical conductivity [16] and the dispersion of the nanoparticles, a few different methods were tried. In addition, the preparation method used to disperse the nanoparticles results in very different surface properties of the nanoparticles. This in turn affects which polymer is used in the nanocomposite. Prior researchers have found that even non-charged particles can be assembled by LbL with the appropriate polymer system [10, 17].

The first preparation method was sonication only [18]. 0.1 g of nanoparticle was added to 100 mL of water and probe tip sonicated for 45 minutes at about 50 W. Nanoparticles prepared in this way were found to assemble well with PAA at a pH=2.5, where PAA is only slightly negatively charged. The method was successfully used to assemble films of CNF and SWCNT. Second is PSS-wrapping [10]. 0.1 g of nanoparticle with 0.2 g of PSS in 100 mL of water were bath sonicated for 2-3 days. This assembled well with PEI at a pH of 10, meaning that the PEI was only slightly positively charged. The PSS-wrapping method worked for CNF and MWCNT, but not very well for SWCNT. The final method was to disperse the nanoparticles using the common surfactant SDS. 0.1 g of nanoparticle was added to 100 mL of a 1% SDS solution with probe tip sonication for 30 minutes at 45 W. This dispersion was then assembled with PDDA, a strong cationic polyelectrolyte. Films were assembled with CNF, but the method did not work as well for MWCNT or SWCNT.

Figure 3 shows SEM micrographs of completed films using CNF with each of the three different methods. Examining the different films, the sonication method appears to result in the poorest dispersion, with fibers closely bundled together. The PSS and SDS methods resulted in better dispersion with more isolated ‘clumps’

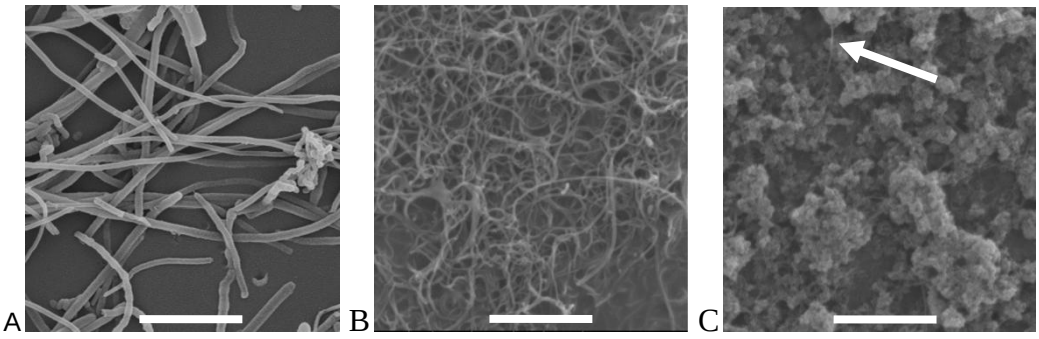

Figure 2. CNF(A), MWCNT(B), and SWCNT(C) all at 40,000X magnification (bar is 2 μm). These Scanning Electron Microscope pictures are of completed films. Note that the SWCNT has a lot of electrically conductive contaminants, though some fibers are also visible (see arrow).

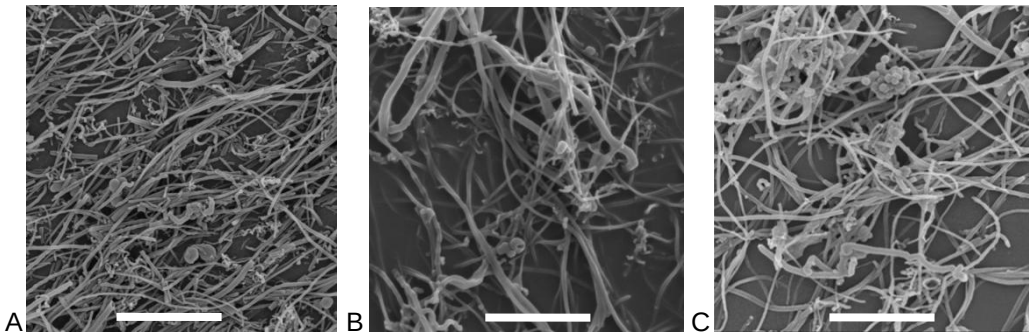

Figure 3. CNF nanocomposites where the CNF were dispersed using (A) pure sonication, (B) PSS wrapping, and (C) SDS surfactant. Note the different levels of fiber bundling and clumping. All three views are at a magnification of 20,000. The bar is 4 μm.

where multiple fibers are connected together. While similar, it may be that the SDS method had more clumps than the PSS-wrapping.

The films were processed using the SSLbL parameters described in Table I for all cases but those with sonication-only preparations. These solutions were not sprayed, but were poured directly onto the spinning disk.

NANOCOMPOSITE MATRIX

Two different nanocomposite matrix types were examined: polymer only and polymer/nanoclay. Polymer/nanoclay films have been shown to have good stiffness and strength properties [15]. By making the matrix stronger and stiffer, the deformation of the conductive nanoparticles is hypothesized to change, with the nanoparticles less able to move around than with the weaker polymer-only matrix. The clay/polymer matrix was formed with a layup of $(CNF/PDDA)_2/(Laponite\ or\ Montmorillonite/PDDA)_2)_x$. SEM micrographs of completed films are displayed in Figure 4.

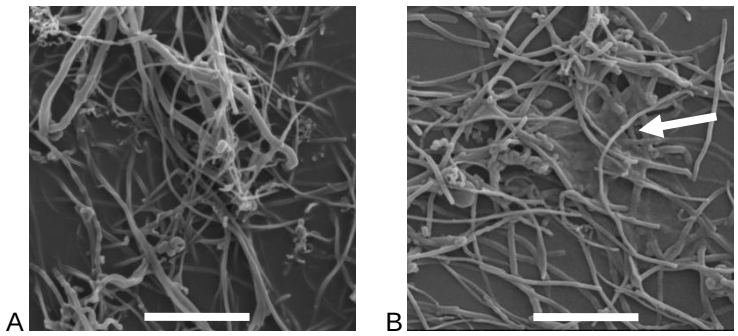

Figure 4. A nanocomposite film with a polymer matrix (A) and a polymer/laponite matrix (B). In this case, the dispersion techniques are by PSS-wrapping and SDS, respectively. Note the matrix bridging of fibers in the clay case. Micrographs are at 20,000 magnification, with the bar as 4 μm.

RESISTANCE-STRAIN RELATIONSHIP

Theoretical

The standard metal foil strain gage is a very simple device. Changing to film strain gages increases both complexity and the possibilities dramatically. First, the deformation in two dimensions affects the measurement, and second, the strain-resistance model becomes more complex. In order to use resistance-strain measurements either as a way to understand the fundamental structure of conductive films or in sensor applications, both of these complexities must be addressed.

RESISTANCE CHARACTERIZATION

Consider a film with anisotropic resistivity. Although some of the nanofilms that have been produced are initially isotropic, the anisotropic case must be considered because even an initially isotropic sample becomes anisotropic when it is deformed [19]. Fortunately, resistivity is a tensor, it is symmetric, and in this case it can be reduced to two dimensions and expressed in the form-

$$[\rho] = \begin{bmatrix} \rho_{xx} & \rho_{xy} \\ \rho_{xy} & \rho_{yy} \end{bmatrix} \tag{2}$$

By aligning the sample in such a way that the material principal axes are oriented with the global coordinate system and dividing by the nanocomposite thickness, the sheet resistance tensor, with the principal sheet resistances, R_2 and R_1 is, ($R_2 > R_1$)

$$[R_s] = \begin{bmatrix} R_1 & 0 \\ 0 & R_2 \end{bmatrix} \tag{3}$$

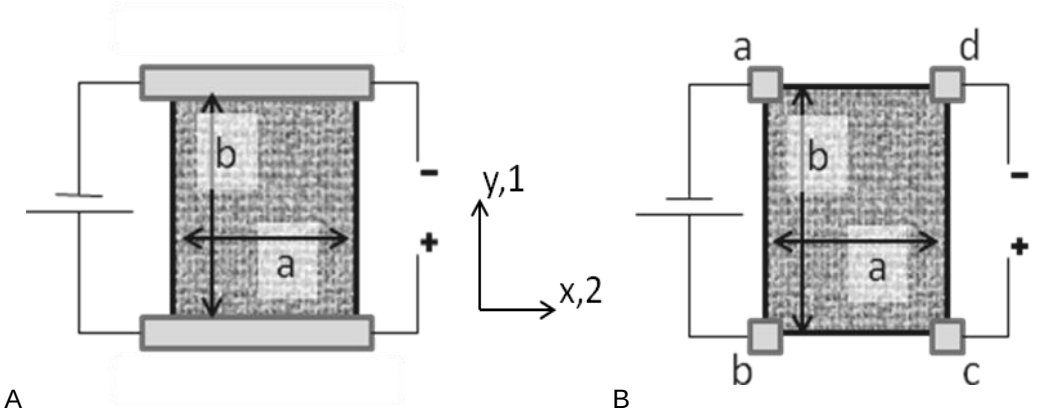

Figure 5. Two common resistance measurement techniques. A is the 'parallel' configuration, and B is the van der pauw configuration.

Characterization of the electrical resistance of a material for a given state of strain can be done in a variety of ways. For a rectangular film, two of the simplest ways to measure sheet resistance are the van der pauw configuration [20] and what will be called here the 'parallel' configuration, both shown in Figure 5. The parallel configuration, in which the electrical contact consists of the entire top and bottom edges is very simple and is commonly used. The resistance is calculated by

$$R' = \frac{V}{I} \tag{4}$$

where V and I are the voltage and current, and R' is the notation used here to signify resistance measured in the parallel configuration.

The van der pauw method is different in that the current is applied at two discrete points and is measured at two other discrete points. The resistance is defined as

$$R_{abcd} = \frac{V_{cd}}{I_{ab}} \tag{5}$$

or the voltage drop from corners c to d for a current flowing from corners a to b, recalling that current flows from negative to positive. The van der pauw method has several advantages. First, connecting to the film is simpler since the contacts are point contacts and the contact resistance is neglected by measuring voltage separately from the point that the current is applied. Second, it is applicable to arbitrarily shaped samples, and third, the measurement includes information about the anisotropic sheet resistance. This comes at the cost of increased complexity. For an arbitrarily shaped, anisotropic sample with infinitesimal contact points, Van der Pauw and others, such as Price [20] showed that:

$$\exp\left(-\pi R_{abcd} \Big/ \sqrt{R_1 R_2}\right) + \exp\left(-\pi R_{bcda} \Big/ \sqrt{R_1 R_2}\right) = 1 \tag{6}$$

where R_{bcda} is defined as in equation (5) and R_1 and R_2 are the principal sheet resistances defined in equation (3).

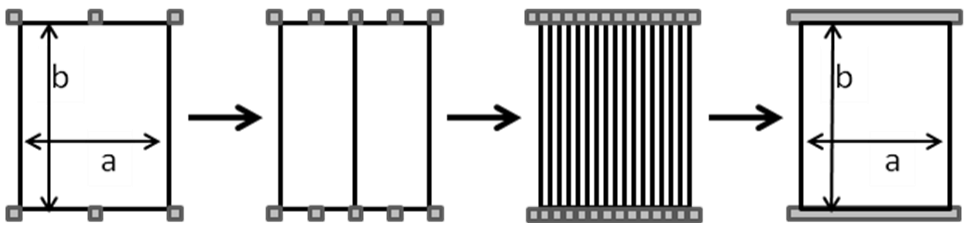

Figure 6. Limiting case as the van der pauw configuration approaches the parallel configuration.

In the case of a rectangular sample aligned with the principal axes as shown in Figure 5, Price showed that

$$R_{abcd} = \frac{-8\sqrt{R_1 R_2}}{\pi} \ln \prod_{n=0}^{\infty} \tanh\left\{ \sqrt{\frac{R_2}{R_1}} \frac{a}{b} (2n+1) \frac{\pi}{2} \right\} \tag{7}$$

and similarly for R_{bcda} by switching every subscript of 1 and 2, as well as dimensions *a* and *b* [20]. Using equations (7), it is possible to numerically solve for R_1 and R_2.

The difference between the van der pauw and parallel configurations can be found by examining the van der pauw measurement more closely. Specifically, the limiting case as *a/b* approaches 0 and the van der pauw measurement approaches the parallel configuration. Start with an alternate van der pauw geometry shown in Figure 6. In this case, the current is applied in the two center probes and measured at either edge. Due to the symmetry of the system, it is possible to subdivide this cell into two identical cells. Each of the two new cells has a width of *a/2*. The total resistance of the two cell body is simply the resistance of two identical resistors in parallel.

Simon defined R_{abcd} for the alternate geometry shown in Figure 6 [21]. Taking the limit of this definition as the number of cells approaches infinity and solving the infinite series, we derive the relationship for the parallel configuration:

$$R = \frac{Rabcd}{N} = \lim_{N\to\infty} \frac{4\sqrt{R_1 R_2}}{\pi} \sum_{n=1,3}^{\infty} \frac{1/N}{n \sinh\left(\sqrt{R_2/R_1} \frac{a/N}{b} \frac{\pi}{2} n \right)} =$$

$$= \frac{4\sqrt{R_1 R_2}}{\pi} \sum_{n=1,3}^{\infty} \frac{1}{\sqrt{R_2/R_1} \frac{a}{b} \frac{\pi}{2} n^2} = \frac{4\sqrt{R_1 R_2}}{\pi} \frac{\pi^2}{\sqrt{R_2/R_1} \frac{a}{b} \frac{\pi}{2} 8} = \boxed{R_1 \frac{b}{a} = R'} \tag{8}$$

which is exactly what would be expected given the definition for sheet resistance. The important conclusions from equation (8) are the similarity between the two methods and an understanding that van der pauw resistance is a function of R_1, R_2, and the geometry, while the parallel resistance is a function only of R_1 and the geometry.

GEOMETRIC EFFECTS

Using the governing equations for the van der pauw and parallel methods, equations (7) and (8), it is possible to evaluate what the measured resistances *R'* or R_{abcd} actually mean in terms of intrinsic material properties. The simplest way to do this is to use the governing equations for the two methods and input characteristic values for R_1, R_2, *a*, and *b*, and then calculate what *R'* and R_{abcd} would

be under those conditions. The strain is initially added just into the length scales such that

$$\frac{b}{a} = \frac{b_0(1+\varepsilon_1)}{a_0(1+\varepsilon_2)} = \frac{b_0(1+\varepsilon_1)}{a_0(1-\upsilon\varepsilon_1)} \tag{9}$$

In order to imitate the experimental test results better, $R'(\varepsilon)$ and $R_{abcd}(\varepsilon)$ can then be translated to the gage factors $GF'(\varepsilon)$ and $GF_{abcd}(\varepsilon)$ by equation (1). This gage factor is a better comparison because it directly measures the sensitivity of a given film and is dimensionless.

Table II shows the effect of geometric properties on the gage factor for both measurement methods. One of the most important effects to note is that the Poisson's ratio of the base material affects the gage factor even for the simple parallel measurement. By taking the derivative of the boxed portion of equation (8) with respect to strain, even assuming R_1 to be constant with respect to strain, it can be seen that the Poisson's ratio effect cannot be removed from the measurement, so the transverse strain will always affect the resistance measured in the principal direction. Thus, for a film strain gage, there is no such thing as a '1-D' measurement.

Another important effect is the film dimensions, *a* and *b*. The gage factor for the parallel method does not change with dimension, since the normalization process removes the dimensional information. Unfortunately, this is not the case for the van der pauw method since the transcendental equation makes it impossible to remove this effect. While it is unfortunate that *a/b* cannot be removed entirely from the gage factor with a single measurement, it is still possible to mitigate the effects. First, by comparing films with similar ratios, quantitative comparisons are still valid. Second, this effect can be analytically removed by using both R_{abcd} and R_{bcda} measurements to solve directly for R_1 and R_2. In this study, the first method will be primarily used.

The final effect is that of the initial anisotropic ratio, R_2/R_1. It is interesting to note that for a sample that is strained in the *2* direction, the sensitivity increases as the transverse resistance increases. In other words, a gage will be more sensitive when tested in the R_1 direction (since R_1 is defined to be less than R_2). Importantly, the actual magnitudes of R_2 and R_1 do not affect the gage factor for either measurement system.

TABLE II. EFFECT OF GEOMETRIC PROPERTIES ON GAGE FACTOR

	GF_{abcd}	GF'
Poisson's = 0.3+/-10%	4.1±8%	1.3±8%
a/b = 1 +/- 30%	4.1±30%	1.3±0%
R_x/R_y = 1.0	4.1	1.3
R_x/R_y = 1/3	2.5 (-38%)	1.3 (0%)
R_x/R_y = 3/1	7.1 (+72%)	1.3 (0%)

MATERIAL STRAIN-RESISTANCE EFFECTS

The principal cause of film sensitivity is the intrinsic sensitivity of the material. Mathematically, the relationship between the second order strain tensor and the second order resistance tensor is a fourth order 'piezoresistivity' tensor. As is the case with the relationship between stress and strain, this 'constitutive' tensor can be simplified using material symmetries and other methods. For example, taking a perfect silicone crystal structure it is possible to identify three unique piezoresistive coefficients [19]. However, for a nanofilm, the problem is more nonlinear.

Figure 7 demonstrates why this is the case. Ideally, the deformation would be as shown in (B) as a uniform deformation of matrix and fibers. Increase in resistivity would be caused by change in resistance due to fibers stretching and changes in the contact zone. However, (C) demonstrates another possibility – a system where fibers are considered much stiffer than the matrix and have structurally weak fiber-fiber connections. In this case, the fibers do not deform, but do translate. The change in resistance would be primarily caused by changes in the percolation path. Interestingly, (C) shows how new contact points can be formed under deformation, resulting in a *decrease* in resistance for an increase in strain. Such a negative gage factor was seen experimentally.

Regardless of the deformation pattern occurring, it should be assumed that both R_1 and R_2 are functions of strain in all three directions. However, to give some indication of how the material sensitivity affects the gage sensitivity, some simplifying assumptions can be made. First, assuming that the strain in the thickness direction has little effect and that the Poisson's ratio is constant for all tests, it is possible to approximate R_1 to be a function of only one strain component. Assuming that this is a linear relationship, the simplest form of gage factor is achieved. Using these simplifying assumptions to give R_1 and R_2 as functions of strain in the governing equations, the effects of the material gage factors on the film gage factor can be shown in Figure 8. From this figure, it can be seen that the *GF'* is affected only by the gage factor in the stretched direction. GF_{abcd} is primarily affected in the same way, but there is a measureable effect from the transverse gage factor. This plot also indicates that for the same materials, the R_{abcd} measurement method is generally more sensitive than the *R'* measurement.

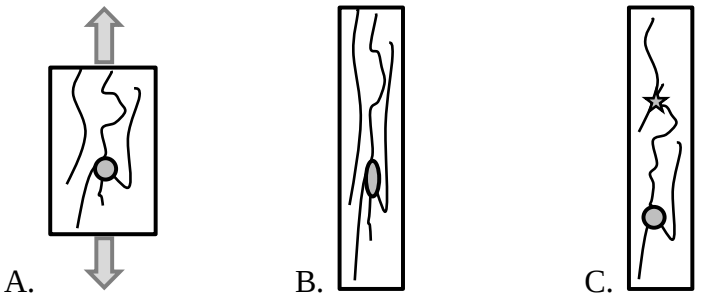

Figure 7. Film under strain. A is the initial configuration, B represents an 'ideal' deformation, while C assumes only loosely attached fibers. The star indicates a new connection point established.

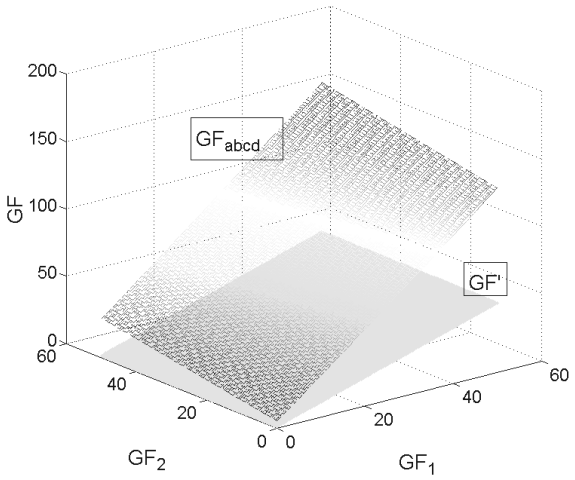

Figure 8. A contour plot of the film gage factor as a function of the material gage factors in the two principal directions. GF_{abcd} is the contour on top.

Strain-Resistance Summary

1. Film strain gages are significantly more complex than one-dimensional wire gages.
2. Regardless of the measurement technique employed, the Poisson's ratio and the intrinsic material sensitivity make the measurement dependent on the strain in both the testing and transverse directions.
3. Using the van der pauw method, it is possible to solve for the sheet resistance in two directions. Although the van der pauw measurement is a more complex measurement of resistance, the method results in a higher sensitivity and includes information from the transverse direction, making it better suited for characterizing an inherently two dimensional system. It is the method used in the experimental portion of this work.

EXPERIMENTAL RESULTS

Procedure

SSLbL can build films on a wide variety of substrates. For this work, the film was deposited directly on a 1.6 mm thick polycarbonate disk (100 mm diameter). The polycarbonate was cleaned with soap and water, and then 5 cycles of (PAA/PEI) were applied followed by the strain gage nanocomposite. After determining the principal resistivity directions of this film, dogbone shaped specimens were cut from the disk such that one dogbone was in the 'major' direction, R_1 and one was in the 'minor' direction, R_2. The actual 'gage' was made by removing the film around the desired gage area on the dogbone. This was done by rubbing with a dampened cotton swab or q-tip. One particular challenge was to electrically connect to the corners of the gage and hold the connection for strains up

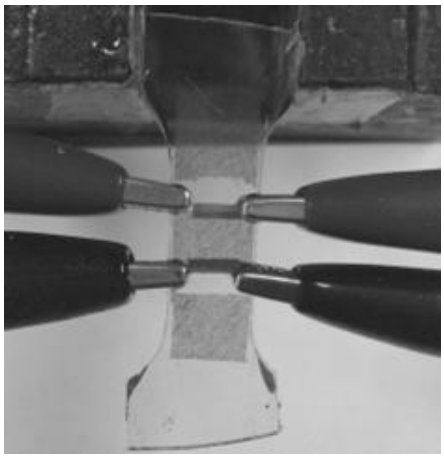

Figure 9. A prepared sample. Note that small 'ears' were left at the corners of the gage, which is where the actual electrical connection is made. On the back of the sample are pieces of reflective tape for use with the laser extensometer. The gage area of the dogbone is approximately 1 cm wide, and the gage itself is about 8.3mm X 6.0mm.

to 5%. Some tests were performed with carbon-based glue, but this glue generally failed at about 1% strain. Conductive grease was also used but resulted in more noise in the measured data as well as some possible film contamination. The most successful method was to use alligator clips to hold ball bearings to each of the four corners. This provided a 'point' contact that did not appear to deteriorate even at high strains. Because the van der pauw configuration is a Kelvin style measurement, contact resistance is not a concern as long as it doesn't increase the overall impedance too much. Figure 9 shows a sample in the final attached configuration.

To characterize the film, a set of R_{abcd} and R_{bcda} measurements were made in the zero strain state. Then the dogbones were tested in a standard servo-hydraulic tensile tester. During the test, the resistance in the testing direction, R_{abcd}, was measured simultaneously with the strain. The strain was measured using a laser extensometer focused with laser tape on the back of the gage. Load was also measured using a 1,000 lbf load cell. In general, maximum load was in the range of 200 lbf. This load was used to check the strain values from the laser extensometer. There were a few tests where the laser data was corrupted and so strain was back-calculated from the load.

In order to gain as much information as possible from each test, the test was not simply an increasing ramp. Instead, it was a series of load-hold-unload ramps. This made it possible to examine not only gage factor, but also the unloading characteristics of the film.

Figure 10 shows a plot of strain vs. time for one of these tests and the corresponding resistance. For all the presented data, the resistance shown is the normalized resistance, or R_{abcd}/R_{abcd_0}. Examining Figure 10B the sensitivity of the material can be seen, as well as the unloading effect. In this case, it appears that beyond a certain strain, the resistance of the film was permanently changed. This is more clearly seen by plotting the resistance against the strain as in Figure 11. The key points that were examined experimentally were the initial strain and the strain

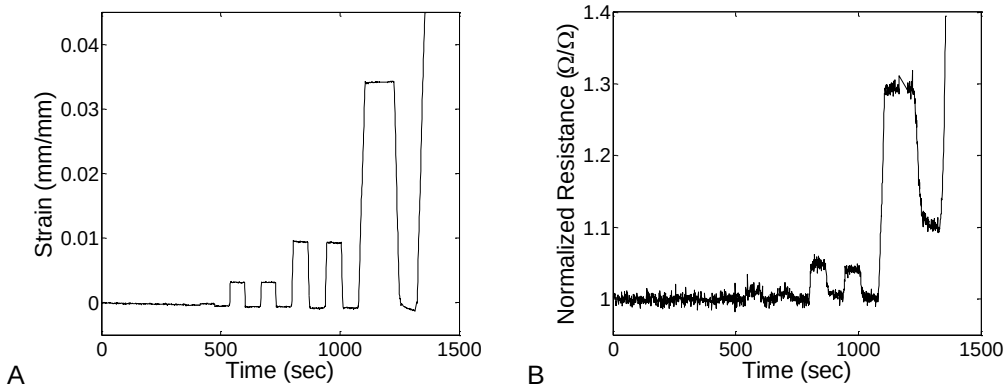

Figure 10. (A) A graph of the strain applied to the sample over time. (B)The normalized resistance, measured over time for the same sample.

at 4%. Some additional information was gained from looking at the hysteresis and the 'irreversible point,' or the strain at which the sample no longer returned to the initial resistance as it returned to the unstrained state. This irreversible point is naturally affected by the coarseness of the strain steps taken, so it is a better qualitative than quantitative value.

Results

Table III summarizes the results for the different film configurations that were produced. Electrical properties of the film are those at zero strain found from the joint R_{abcd}, R_{bcda} measurements. These include the anisotropic sheet resistance $\sqrt{R_1 R_2}$ and the anisotropic ratio R_2/R_1. The different nanoparticle preparations are

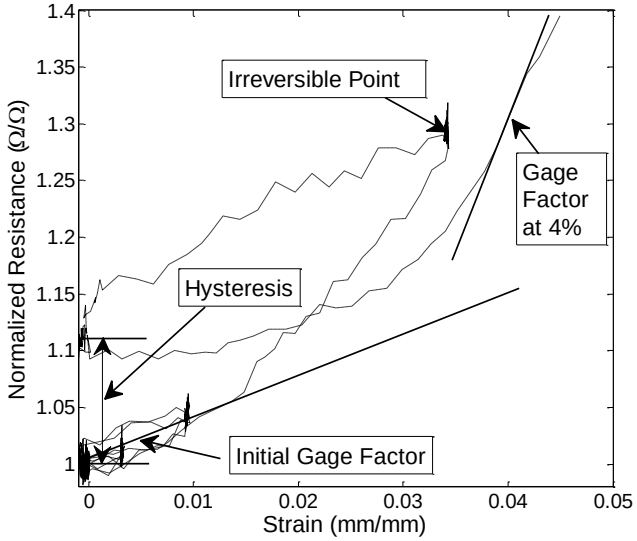

Figure 11. Typical normalized resistance vs strain plot with the principal information noted.

TABLE III Gage Factor Results

General Properties						Gage Factor			
						Major Axis		Minor Axis	
#	Fiber	Prep	Matrix	$\sqrt{R_1R_2}$ (KΩ)	R_2/R_1	0%	4%	0%	4%
1	CNF	Son	P	25±3.7	3.2±0.7	13	1560	8	205
2	CNF	Son	P	8.7±0.2	2.6±0.1			7	43*
3	CNF	SDS	P/M	6.1±0.4	1.7±0.2	6	31	4	21*
4	CNF	PSS	P	26±8.7	1.6±0.8	1	20	1	21
5	CNF	SDS	P/L	7.7±0.7	1.6±0.2	5	2.5	2	18
6	SWCNT	Son	P	11±1.4	1.8±0.3	4	51*	3	9
7	MWCNT	PSS	P	17	1.3			3	3

*The test was stopped before 4% strain was reached due to a loss of electrical connection with the film. The value shown is the final sensitivity.

abbreviated here as 'Son' meaning sonication only, and 'SDS' or 'PSS' referring to the dispersion agent. The matrix is either polymer only (P), polymer/montmorillonite (P/M), or polymer/laponite (P/L). The major and minor axis results refer to testing in both the 1 and the 2 resistance directions as already explained.

DISCUSSION

Gage Factor

For this group of films, the highest gage factor was case 1, with an initial factor of 13 and a very unique 4% factor of 1560. Using the mathematical model explained before, with an assumed material gage factor of 1 in both directions and with the measured R_1/R_2 and a/b for the films, the gage factor predictions would be 15 and 24 for the major test and 4.3 and 4.6 for the minor test. So, the material anisotropy does play a role, especially initially. However, this is insufficient to explain the higher minor axis gage factor and the significant increase in the gage factor at higher strains. Examining a micrograph of the (CNF_sonication/P) films in Figure 3A and comparing it with the other micrographs, there are a few obvious differences. It appears that the pure sonication mixing results in fibers that are not as fully dispersed, but instead are heavily bundled. They also appear to be more aligned. This greater anisotropy is quantified in the higher values of R_s/R_1 for cases 1 and 2.

Although case 1 and case 2 have an identical fiber and matrix and a similar anisotropic ratio, they have a different gage factor. This is partly because case 2 was only strained to about 1.15%. The test used carbon glue to make the electrical connections, and the carbon glue failed at that point. Still, case 1 had a gage factor of about 83 at 1% strain, roughly double the gage factor of case 2. The material difference between the two films is that they were manufactured with different thicknesses, seen in the sheet resistance values. It is possible that, particularly in

the limit of a very thin film, the percolation network has some thickness dependence. Considering a percolation-only theory of resistance, it could be considered that loss in percolating points in the plane could be partially compensated by continuity in the thickness direction. It is known that LbL films have a high degree of interdigitation in the layers, so such a 3D effect is not surprising [9]. Together, this implies that the higher gage factor in case 1 is a function of the strong anisotropy, bundled fibers, and a thin film limiting 3D percolation.

Matrix Effect

Case 3 and case 5 had a 'clay' matrix with a $((CNF/PDDA)_2/(Clay/PDDA)_2)_x$ layup. The large size of the CNF means that the polymer and laponite were likely able to diffuse down into the gaps created by the CNF [22]. Case 5, with laponite nanoclay appears to have had excellent bonding. A cross section of case 5 is shown in Figure 12. The film was damaged in the cross sectioning, serendipitously demonstrating the matrix-CNF bonding. Montmorillonite, a much larger clay platelet, probably did not diffuse in as well as laponite, resulting in a lower quality matrix-fiber connection and possibly creating voids as well.

The effect that the clay matrix compared to a polymer matrix can be seen by comparing cases 4 and 5 because they have roughly similar CNF structures, seen both in Figure 4 and in the identical anisotropic ratios. However, there are stark differences seen by examining the resistance-strain traces in Figure 13. From Figure 13 the differences between the clay and the polymer matrix are most obvious in the portions of the curve where the strain is constant or unloading. The behavior of the polymer matrix film is very interesting because the resistance reduces MORE than it gains as it is held at a constant strain or unloaded. In others words, this is a 'reverse' strain gage that increases in conductivity for different strains. The proposed explanation for this is similar to the explanation shown in Figure 7 above with a soft matrix and structurally weak fiber-fiber connections. As the sample is strained, the fibers move around into other configurations, aligning in the strain direction and resulting in more efficient percolation. It is important that the

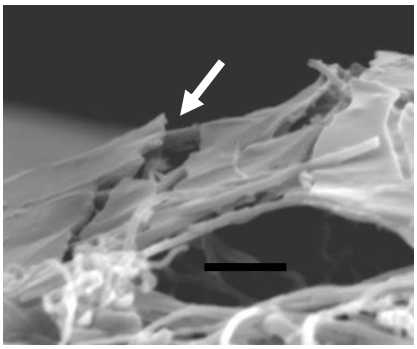

Figure 12. SEM view of a damaged CNF/clay-laponite film. The arrow highlights broken CNF fibers demonstrating good fiber-matrix connectivity. The bar is 1 μm.

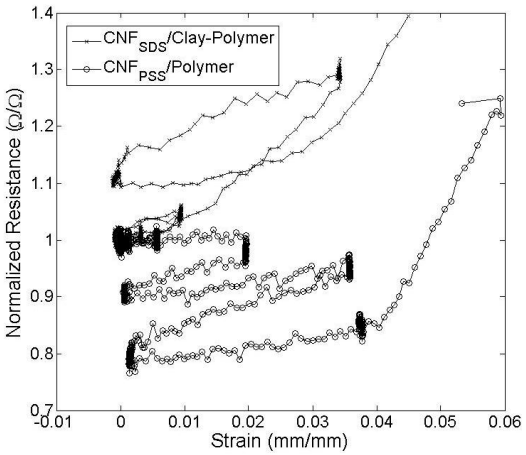

Figure 13. Normalized resistance vs strain for a clay matrix and a polymer matrix films.

resistance does still increase as the film is loaded, implying this effect is primarily due to a relaxation type of behavior. The clay nanocomposite appears similar in the SEM, but the clay matrix appears to prevent the relaxation process by locking the fibers in the original configuration

The hysteresis in the clay matrix case at higher strain can be assumed to come from permanent damage to the film, in which case percolation pathways that existed initially are lost, resulting in an increased resistance when returning to zero strain. The fact that similar negative gage-factor behavior didn't occur with the other polymer systems implies that the smaller nanotubes bond more strongly than the large CNF and that the sonication preparation results in nanofibers being more tightly held together.

Conductive Nanoparticle

The SWCNT and MWCNT films had lower gage factors than their CNF counterparts, but with greater linearity over a larger strain range. Figure 14 shows the R_{abcd} vs Strain trace for these, measured in the minor direction. Noting the significantly more linear behavior, the simple model developed above was fit using the measured geometric and resistance information. Using this, the SWCNT model fit best with GF_2=4.0, GF_1=1.0. The MWCNT was best fit with GF_2 = -0.8, and GF_1 = 0.5.

The structural differences in these films include a different conductivity of the nanoparticle, since the resistance of a SWCNT, MWCNT, and CNF can all be expected to differ and different percolation characteristics. From Figure 2 it can be seen that the MWCNT structure is more tangled and the fibers are more curved than the CNF films, which is reflected in the nearly isotropic initial condition.

Why this results in the different strain behavior is more difficult to explain. It is possible that the greater entanglement together with stronger fiber-matrix interactions caused by the increased surface area of nanoparticles might result in a displacement that is characterized by less fiber-fiber motion disrupting percolation

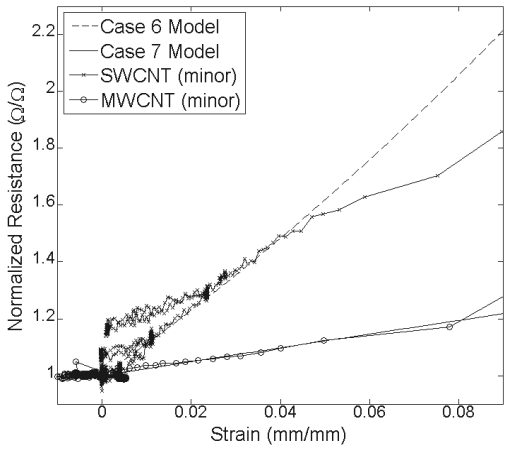

Figure 14. Normalized resistance vs strain for the case of SWCNT and MWCNT films. The mathematical model developed above is also shown.

networks and more by the kind of deformation postulated in Figure 7B. This is supported by the material gage factors used in the fitting model. The low material sensitivity values, particularly in the MWCNT case imply that the film gage factor is more strongly influenced by geometric than intrinsic material piezo-resistance effects.

CONCLUSIONS

- SSLbL, a variation of LbL, is a robust method capable of manufacturing a wide variety of different nanocomposites, allowing for direct comparisons of the structure-property relationships.
- Film strain gages are inherently more complex than traditional wire gages, with 2D strain and material effects making it more difficult to relate measured resistance with intrinsic material properties. However, the greater complexity also gives advantages in the information that can be gained from a single measurement.
- The Van Der Pauw method of measuring film resistance is a good way to gain deeper insights into the two dimensional resistance of anisotropic films.
- A CNF nanocomposite with very high values of GF_{abcd} = 13-1560 (ε=0-4%) was developed. This was made by using a sonication-only preparation of CNF, resulting in bundles of aligned CNF being deposited in the nanocomposite.
- Clay matrix nanocomposites can be manufactured with good CNF-clay connectivity. It appears that the clay keeps the nanoparticles from relaxing or rearranging in the film during constant strain or unloading.
- Nanotube strain gages appear to be more linear than CNF gages, but are not as sensitive.

Future work should focus on using the best results from these films to further improve strain gage properties. For example, by repeating case 1 with a clay

matrix, it may be possible to develop a gage with good unloading characteristics but still with very high sensitivity. Also, none of the gages presented 'failed' during the test. The tests were always stopped by either the substrate or the electrical contact failing. So, the ultimate strain of these gages has not been determined. Since several advanced applications would require gages with very large strain-to-failure, this is an important aspect which has not yet been sufficiently explored for these materials.

ACKNOWLEDGEMENTS

The authors gratefully acknowledge support from Indiana's Center for Advanced Manufacturing. M. Merrill expresses appreciation for a GAANN training grant. They also thank Debby Sherman in Purdue's Life Sciences Microscopy for her assistance with the SEM images.

LIST OF REFERENCES

1. Loh, K. J., Lynch, J. P. & Kotov, N. A. 2006. "Mechanical-electrical Characterization of Carbon-Nanotube Thin Films for Structural Monitoring Applications," presented at the Smart Structures and Materials 2006 Conference, Feb 27-Mar 2, 2006.
2. Park, M. 2007. "Deformation Dependent Electrical Resistance of MWCNT Layer and MWCNT/PEO Composite Films," Dissertation. Purdue, West Lafayette.
3. Dharap, P., Li, Z., Nagarajaiah, S. & Barrera, E. V. 2004. "Nanotube Film Based on Single-Wall Carbon Nanotubes for Strain Sensing," *Nanotechnology* 15, 379-382.
4. Lalli, J. H., Hill, A., Goff, R., Claus, R. & Arregui, F. 2005. "Nanostructured Sensors," presented at the 2005 IEEE Sensors Conference, Oct 30-Nov3, 2005.
5. Li, X. & Levy, C. 2007. "Multi-Walled Carbon Nanotube Film as Strain Sensors for Structural Vibration Control," presented at the 2007 NSTI Nanotech Conference, May 20-24, 2007.
6. Reale, A. et al. 2004. "Evaluation of the Gauge Factor for Membranes Assembled by Single-Walled Carbon Nanotubes," *Applied Physics Letters* 85, 2812-2814.
7. Zhang, W., Suhr, J. & Koratkar, N. 2006. "Carbon Nanotube/Polycarbonate Composites as Multifunctional Strain Sensors," *Journal of Nanoscience and Nanotechnology* 6, 960-964.
8. Loh, K. J., Junhee, K., Lynch, J. P., Kam, N. W. S. & Kotov, N. A. 2007. "Multifunctional Layer-by-Layer Carbon Nanotube-Polyelectrolyte Thin Films for Strain and Corrosion Sensing," *Smart Materials and Structures* 16, 429-38.
9. Decher, G. 1997. "Fuzzy Nanoassemblies: Toward Layered Polymeric Multicomposites," *Science* 277, 1232-1237.
10. Shim, B. S. et al. 2007. "Integration of Conductivity, Transparency, and Mechanical Strength into Highly Homogeneous Layer-by-Layer Composites of Single-Walled Carbon Nanotubes for Optoelectronics," *Chemistry of Materials* 19, 5467 - 5474.
11. Lin, Y.-H., Jiang, C., Xu, J., Lin, Z. & Tsukruk, V. V. 2007. "Sculptured Layer-by-Layer Films," *Advanced Materials*, 19, 3827-3832.
12. DeLongchamp, D. M. & Hammond, P. T. 2004. "Highly Ion Conductive Poly(ethylene oxide)-Based Solid Polymer Electrolytes From Hydrogen Bonding Layer-by-Layer assembly," *Langmuir* 20, 5403-5411.
13. Guldi, D. M. et al. 2006. "CNT-CdTe Versatile Donor-Acceptor Nanohybrids," *Journal of the American Chemical Society* 128, 2315-2323.
14. Podsiadlo, P. et al. 2005. "Layer-by-Layer Assembly of Nacre-Like Nanostructured Composites with Antimicrobial Properties," *Langmuir* 21, 11915-11921.
15. Podsiadlo, P. et al. 2007. "Ultrastrong and Stiff Layered Polymer Nanocomposites," *Science* 318, 80 - 83.

16. Kotov, N. A., Dekany, I. & Fendler, J. H. 1996. "Ultrathin Graphite Oxide-Polyelectrolyte Composites Prepared by Self-Assembly: Transition Between Conductive and Non-conductive States," *Advanced Materials* 8, 637 - 641.
17. Yang, S. Y. & Rubner, M. F. 2002. "Micropatterning of Polymer Thin Films with pH-Sensitive and Cross-linkable Hydrogen-Bonded Polyelectrolyte Multilayers," *J. Am. Chem. Soc.* 124, 2100-2101.
18. Yang, D.-Q., Rochette, J.-F. & Sacher, E. 2005. "Functionalization of Multiwalled Carbon Nanotubes by Mild Aqueous Sonication," *Journal of Physical Chemistry B* 109, 7788-7794.
19. Mian, A., Suhling, J. C. & Jaeger, R. C. 2006. "The van der Pauw Stress Sensor," *IEEE Sensors Journal* 6, 340 - 56.
20. Price, W. L. V. 1973. "Electric Potential and Current Distribution in a Rectangular Sample of Anisotropic Material with Application to the Measurement of the Principal Resistivities by an Extension of van der Pauw's Method," *Solid-State Electronics* 16, 753 - 762.
21. Simon, S. H. 1999. "Comment on 'Evidence for an Anisotropic State of Two-Dimensional Electrons in High Landau Levels,'" *Phys. Rev. Lett.* 83, 4223.
22. Shim, B. S., Starkovich, J. & Kotov, N. 2006. "Multilayer Composites from Vapor-Grown Carbon Nano-Fibers," *Composites Science and Technology* 66, 1171-1178.